ACS Catalysis

pubs.acs.org/acscatalysis Research Article

Cu Oxamate-Promoted Cross-Coupling of α-Branched Amines and Complex Aryl Halides: Investigating Ligand Function through Data Science

Adrian D. Matthews,[§] Ellyn Peters,[§] John S. Debenham, Qi Gao, Maya D. Nyamiaka, Jianping Pan, Li-Kang Zhang, Spencer D. Dreher, Shane W. Krska, Matthew S. Sigman,* and Mycah R. Uehling*

Cite This: *ACS Catal.* 2023, 13, 16195−16206 Read Online

ACCESS | Metrics & More | Article Recommendations | Supporting Information

ABSTRACT: Synthesis of α-branched aryl amines is a continuing challenge in synthetic and medicinal chemistry. Although transition-metal-promoted C−N cross-coupling is a desirable approach to the synthesis of α-branched aryl amines, there are limited examples of methods that demonstrate broad generality and applicability using structurally complex substrates. Herein, we report a method to cross-couple α-branched amines and aryl halides promoted by Cu using an oxamate ligand system. The method is compatible with many druglike aryl halides and amines and can be executed using miniaturized high-throughput experimentation (HTE) techniques that enable the rapid production of high-quality, consistent data sets. In addition to exploring the substrate scope and executing late-stage library synthesis of an active pharmaceutical, we used miniaturized HTE to interrogate the performance of a library of ligands across multiple substrate combinations in parallel at multiple time points. The data were used to build statistical models that provided insight as to what ligand features are important for function, which further enabled the design of ligands with improved reaction performance.

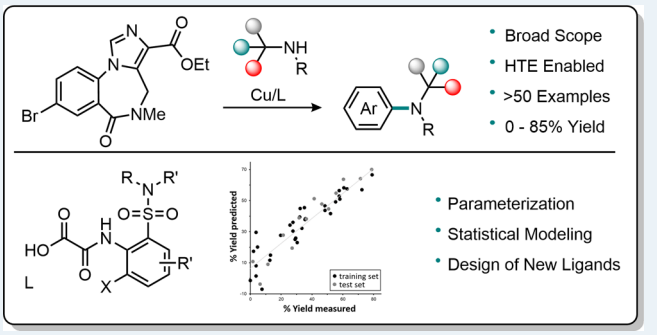

KEYWORDS: *data science, HTE, ligand design, copper, hindered amine cross-coupling*

INTRODUCTION

The incorporation of α-branched aryl amine (αBAA) substructures in pharmaceutically active molecules can impart beneficial changes in lipophilicity, solubility, conformation, selectivity, and activity compared to nonbranched structures.[1−5] As such, a range of methods for the preparation of αBAAs have been developed.[6−14] For drug discovery applications, the C−N cross-coupling of aryl halides and branched amines is particularly useful for preparing diverse αBAAs due to the commercial availability of large pools of building blocks.[15] In its modern form, C−N cross-coupling has a broad scope and is operationally simple,[16−19] but relatively few examples of C−N cross-coupling using α-branched amines have been reported,[20−24] particularly with complex, medicinally relevant substrates. While several studies have focused on Ni- and Pd-catalyzed cross-coupling of primary[25−30] and secondary[29−34] α-branched amines and aryl halides, this transformation remains under-developed for pharmaceutical applications (Figure 1A).

Faced with this challenge, we aimed to explore Cu-based approaches to expand the scope of pharmaceutically relevant C−N coupling reactions involving α-branched amines. In this regard, we were inspired by the oxamate-based ligand class originally developed by Ma and co-workers that has enabled the use of Ullmann-type reactions for druglike aryl halides.[17,35] For example, ligands **L1**−**4** promote the coupling of an unbranched secondary amine, piperidine, with a set of informer aryl halides that represent druglike compounds in relatively high yield (Figure 1B).[35] In terms of Cu-catalyzed cross-coupling of α-branched amines and aryl halides, Shekar and Cook reported a study on the cross-coupling of hindered aryl iodides with α-branched amines using a pyrrole-ol ligand,[36,37] and the Buchwald lab recently reported a novel diamine ligand system to promote such couplings at reduced temperature.[38] These elegant studies represent the state-of-the-art in Cu-catalyzed cross-coupling of α-branched amines

Received: September 25, 2023
Revised: November 10, 2023
Accepted: November 15, 2023
Published: December 5, 2023

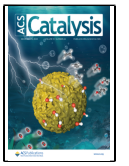

https://doi.org/10.1021/acscatal.3c04566
ACS Catal. 2023, 13, 16195−16206

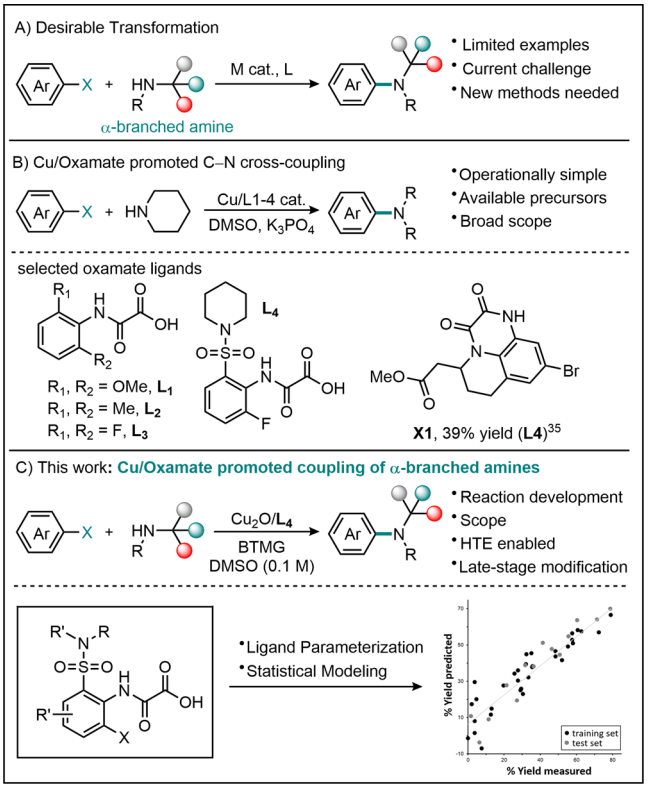

Figure 1. (A) α-Branched amine aryl halide cross-coupling. (B) Cu/oxamate-promoted C−N coupling. (C) Cu/oxamate-promoted coupling of α-branched amines and aryl halides.

and aryl halides. In contrast, while there are isolated reports,[39−42] there have been no systematic studies describing the use of oxamate ligands to promote this transformation.

With our emphasis on drug discovery applications, we further endeavored to develop conditions translatable to miniaturized high-throughput experimentation (HTE) workflows.[43−45] Because HTE approaches generally produce consistent, comparable data sets, they offer several advantages such as material sparing, plate-based reaction optimization[46] and rapid compound library synthesis across multiple scales: traditional parallel medicinal chemistry, microscale,[47−50] and nanoscale syntheses.[51,52] HTE-enabled methods are also ideal for application in direct-to-biology compound profiling, which can vastly accelerate the design-make-test-analyze cycle.[53−56]

In addition, the high-quality data sets generated by HTE facilitate the use of statistical modeling techniques.[57−62] Such tools can be leveraged to interrogate which features of the ligand dictate reactivity and can thus inform the design of future ligands. Despite these advantages, it is relatively uncommon for C−N cross-coupling methods to be optimized for HTE compatibility,[16] which may require the use of high boiling, polar solvents, and relatively dilute conditions (0.1 M or less).

Herein, we report the development of Cu-promoted cross-coupling of α-branched amines and aryl halides employing oxamate ligands. The HTE compatibility of these conditions, combined with the modular nature of the oxamate ligands, facilitated the exploration of the ligand structure−reactivity relationships. Application of statistical modeling approaches to these data sets uncovered ligand features associated with more efficient reactions (Figure 1C). Furthermore, the optimized conditions allowed for broad substrate scope with complex amine and aryl halide coupling partners, enabling applications such as late-stage modification of drugs and medicinal compound library synthesis.

Table 1. Development of Reaction Conditions

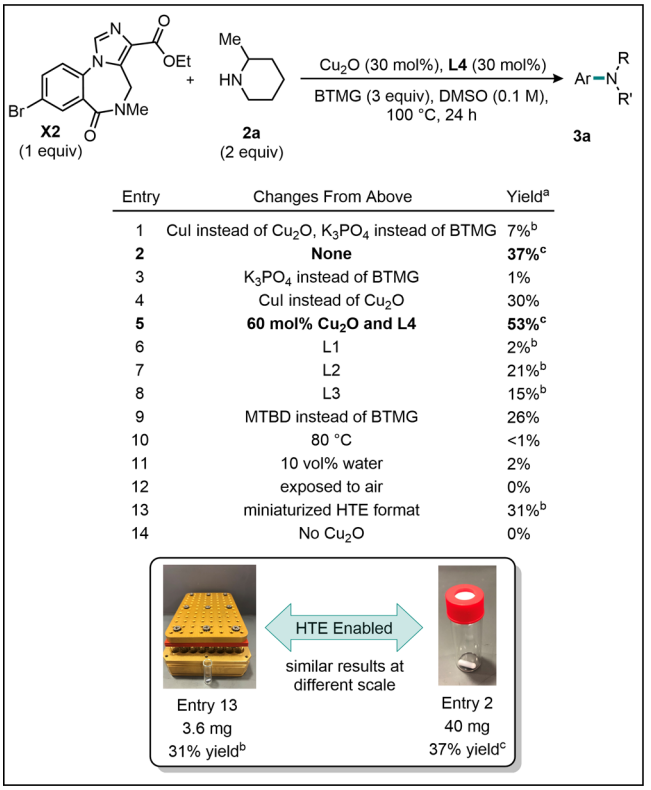

Entry	Changes From Above	Yield[a]
1	CuI instead of Cu_2O, K_3PO_4 instead of BTMG	7%[b]
2	**None**	**37%[c]**
3	K_3PO_4 instead of BTMG	1%
4	CuI instead of Cu_2O	30%
5	**60 mol% Cu_2O and L4**	**53%[c]**
6	L1	2%[b]
7	L2	21%[b]
8	L3	15%[b]
9	MTBD instead of BTMG	26%
10	80 °C	<1%
11	10 vol% water	2%
12	exposed to air	0%
13	miniaturized HTE format	31%[b]
14	No Cu_2O	0%

[a]0.1 mmol scale. [b]0.01 mmol scale. [c]Average of three runs.

RESULTS AND DISCUSSION

We began our study focused on the cross-coupling of informer **X2**[35] and 2-Me-piperidine (**2a**). We initially evaluated previously reported conditions (CuI/**L4**/K_3PO_4) used to cross-couple unbranched amines with informer halides[35] but found these resulted in low yields of the desired product (Table 1, entry 1). After exploration of bases and Cu sources,[63] we recognized that the combination of BTMG, Cu_2O, and **L4** was effective at providing the product in modest yield (Table 1, entry 2). We note that the use of both BTMG and Cu_2O is important for coupling (Table 1, entries 3 and 4). Additionally, we found conversion could be enhanced by increasing Cu and ligand loading; in practice, we routinely employ 60 mol % Cu_2O and **L4** for challenging transformations (Table 1, entry 5). **L4** outperformed several other oxamate ligands evaluated (Table 1, entries 6−8; *vide infra*). Other strong organic bases also promoted the reaction (Table 1, entry 9), but we prefer BTMG as it is relatively mild, widely available, and inexpensive.[64] Like most other Cu-promoted C−N couplings,[17] the reaction required high temperatures (Table 1, entry 10) and was sensitive to the presence of water and oxygen (Table 1, entries 11 and 12). We also investigated how the chemistry translated from preparative medicinal chemistry scale in a 4 mL vial (40 mg,

https://doi.org/10.1021/acscatal.3c04566
ACS Catal. 2023, 13, 16195−16206

Table 2. Ligand Library Prepared to Understand Ligand Function through Parametrization and Statistical Modeling

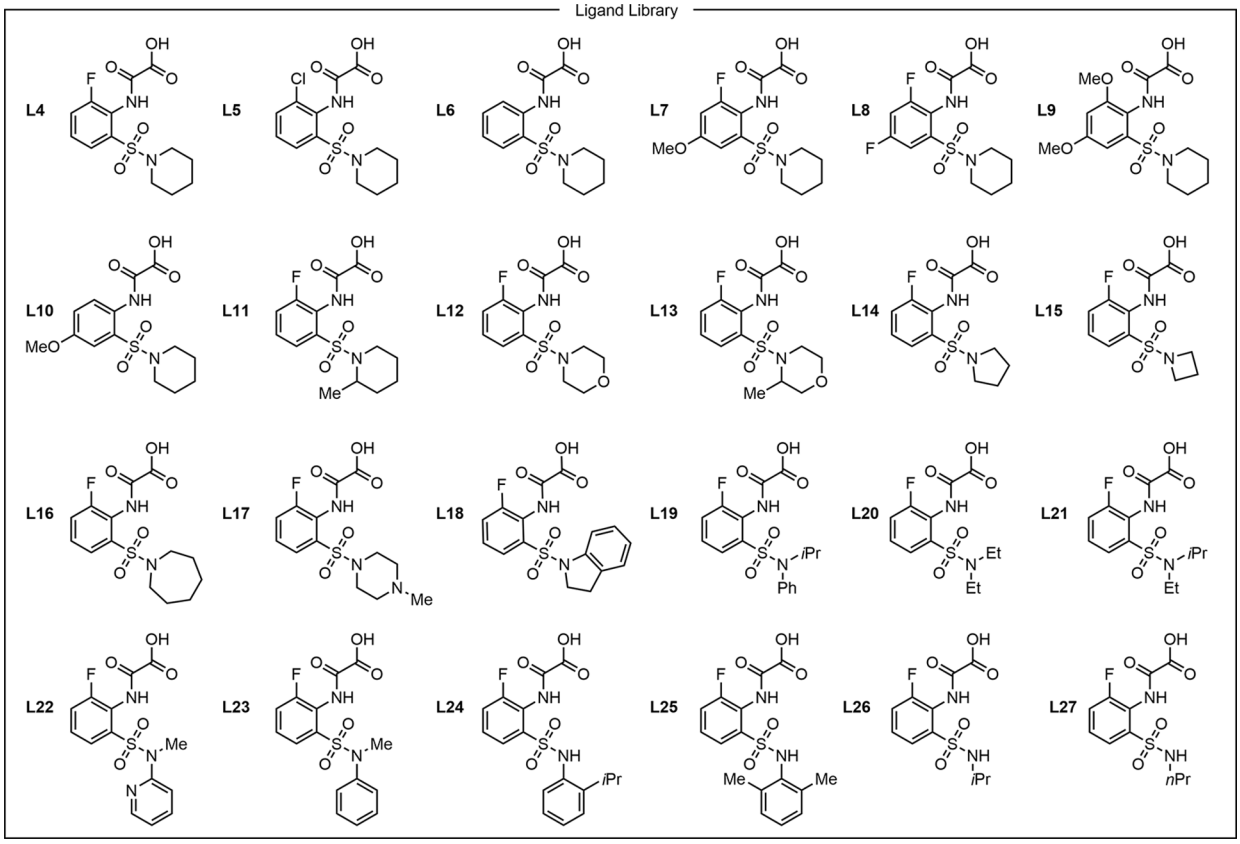

0.1 mmol; Table 1, entry 2) to a miniaturized HTE scale (3.6 mg, 0.01 mmol; Table 1, entry 13) in a 96-well plate. We observed similar yields across these scales, although careful dosing of Cu_2O as a suspension in DMSO was required to obtain reproducible results.[63]

Evaluation of Ligands and Statistical Modeling. Following initial reaction optimization, we sought to better understand the effects of the ligand structure on reactivity and use this insight to improve reaction performance and generality. Based on our initial survey of ligands (Table 1, entries 2, 6−8), we synthesized a library of new oxamate ligands that present an array of structural features designed to systematically interrogate and expand upon structural elements found in **L4**.[63] Specifically, we synthesized and evaluated oxamate analogues that varied the phenylene backbone (Table 2) by introducing one or more methoxy (**L7**, **L9**−**10**), chloro- (**L5**), or fluoro- (**L8**) functional groups, and also exchanging the fluoro group of **L4** with a hydrogen atom (**L6** and **L10**). These changes explored the necessity of a substituent ortho to the oxamate functional group as well as the outcome of perturbing the electronic structure of the ligand. We also designed a series of ligands (**L11**−**27**) with diverse sulfonamide substitutions and the same *ortho*-fluorophenylene backbone of **L4**. These changes were devised to alter both the steric and electronic profiles of the ligand, thus providing a diverse set of oxamate-based ligands to enable a statistical modeling campaign.

Using our validated HTE protocol, we tested the performance of these 23 new ligands alongside **L4** as a positive control in the C−N cross-coupling of 3-bromo-5-phenyl-pyridine (**1a**) with two different model amines, the primary amine 2-Me-1-NH_2-cyclohexane (**2b**) and the secondary amine CBz-protected 2,5-diazabicyclo[2.2.1]-heptane (**2c**), under standard conditions in a 96-well plate reactor (Figure 2). Figure 2A displays the yield of the two corresponding *N*-arylated amine products from **2b** and **2c** as a function of ligand at 3.5 h (average of three runs).[58] To our surprise, the response surface as a function of the ligand was similar across the two amines. In other words, the ligands had the same general rank order when organized by yield. Noting that ligand reactivity trends were consistent, we hypothesized that the data collected for both substrates could be analyzed simultaneously to produce a single model relating yield to ligand features.[63]

An overview of our model building workflow is depicted in Figure 2B. With the empirical data relating the ligand structure to yield (Figure 2A), we next set out to build a computationally derived descriptor set. Ligand conformer ensembles were obtained via a conformational search using CREST at the GFN2-xTB level of theory, followed by density functional theory optimization [M06/6-31+G(d,p)].[57,65−71] Single point calculations were then conducted to obtain molecular descriptors of interest (M06/def2-TZVP).[72,73] A variety of molecular descriptors were extracted from these optimized structures to be used in statistical modeling, including steric measurements (e.g., sterimol values), global electronic terms (e.g., polarizability), and local electronic features [e.g., natural bond orbital (NBO) charges].[74,75] The experimental data points were matched to the corresponding computed ligand features as well as a final numerically

https://doi.org/10.1021/acscatal.3c04566
ACS Catal. 2023, 13, 16195−16206

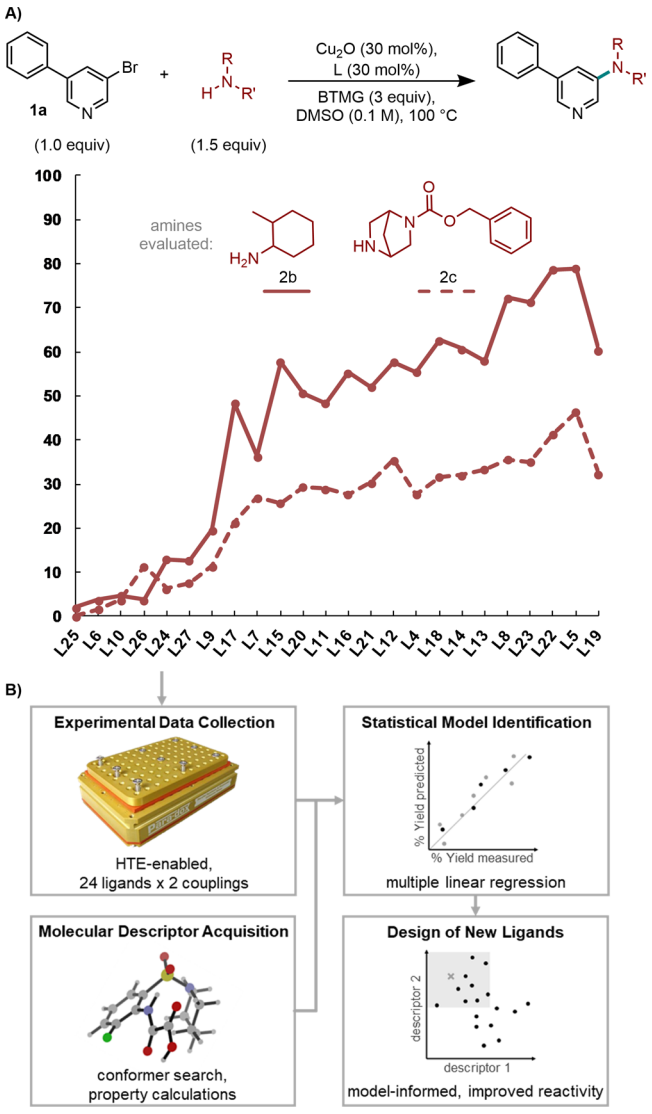

Figure 2. (A) Reaction yield as a function of the ligand at 3.5 h reaction time, average of three runs, and ligands ordered by average yield across both product couples. Solid line indicates products from **2b**, while the dashed line indicates products from **2c**. (B) Modeling workflow overview.

encoded parameter in the form of a 1 or 0 to indicate which amine was used in the reaction. The resulting library was split into a training set (34 data points) and a test set (14 data points) using a pseudo-random algorithm and was subjected to linear regression analysis.[76]

A statistical model was identified, revealing a correlation between the measured reaction yield and the NBO charge of the oxamate nitrogen atom and the NBO charge of the sulfonamide oxygen atoms (Figure 3A). The model further includes a binary substrate classification term, which balances the reactivity differences inherent to the amine identity. With an R^2 of 0.80 indicating a good correlation, internal (Q^2 = 0.73, 5-fold = 0.72) and external ($_{test}R^2$ = 0.92) validations were also used to evaluate the robustness of the model. These metrics are collectively indicative of a robust model.[77−81] The model likewise maintains similar statistics with alternative training-test splits, indicating that the performance of this model is robust and not dependent on training set selection.

Prior to modeling these data, we noted qualitatively that secondary sulfonamide ligands perform worse than tertiary sulfonamide ligands. We also observed that the presence of a halide substituent ortho to the oxamate on the phenylene backbone is critical for an effective reaction, with ligands bearing unsubstituted ortho positions giving reduced yields. Upon removing ligands with both structural features (see Table 2, examples **L6** and **L27** for representative ligands of each type), the model's accuracy increases (R^2 = 0.91) (Figure 3B).

To obtain an accurate measure of relative reactivity across the ligand set, we initially opted to measure and model the yield at an early time point (3.5 h). We next sought to interrogate if the same ligand descriptors that successfully modeled reactivity at the 3.5 h time point also correlated reactivity throughout the course of the reaction. As such, we collected additional yield data for the same set of ligands and substrates at 1 and 21 h time points. Subjecting these data sets to the statistical modeling workflow revealed that the same descriptors adequately described the reaction at each time point (Figure 3C,D). The most statistically sound models were found at 3.5 h, but the same two NBO descriptors are also able to sufficiently capture the trends in the data at 1 and 21 h, indicating that the relative reactivity of each catalyst remains generally constant throughout the reaction and that these models may reflect the relative reaction rate.

The coefficients and identities of the descriptors in the model can be interpreted to gain insight into the feature importance and ligand role in the overall reaction rate. Aside from the descriptor denoting amine identity, the largest descriptor coefficient belongs to the NBO(N) term and has a negative value, indicating generally that the yield is improved with a lower NBO charge on the oxamate N. The presence of this term in the model may be indicative of this moiety engaging in an interaction with Cu, as has been previously suggested for the oxamate ligand class.[42,82,83] The positive coefficient value for the NBO(O) term is indicative of a general trend of greater NBO(O) charges on the sulfonamide O improving yields, and its presence in the model emphasizes the importance of the sulfonamide scaffold in these ligands. It may also indicate that an influential interaction occurs between SO_2 of the sulfonamide and Cu or another reaction component. A larger (in magnitude) coefficient for the NBO(N) term in each of the models suggests that this interaction is more influential than any postulated interaction with the SO_2 of the sulfonamide in determining the yield. However, the change in relative magnitude between the two descriptors from the original model (Figure 3A) to the model omitting the ligands without halide substitution on the phenylene backbone (Figure 3B) demonstrates a clear effect of halide substitution. When these ligands are removed, the coefficients of each term are similar, suggesting that the NBO(N) term is sensitive to halide substitution on the arene, and rendering these moieties equally important in governing reactivity. Finally, we can inspect the relative importance of the features across the time points measured in this reaction and ascertain that because the relative feature importance does not shift throughout the reaction, the mechanism is likely consistent throughout.

https://doi.org/10.1021/acscatal.3c04566
ACS Catal. 2023, 13, 16195−16206

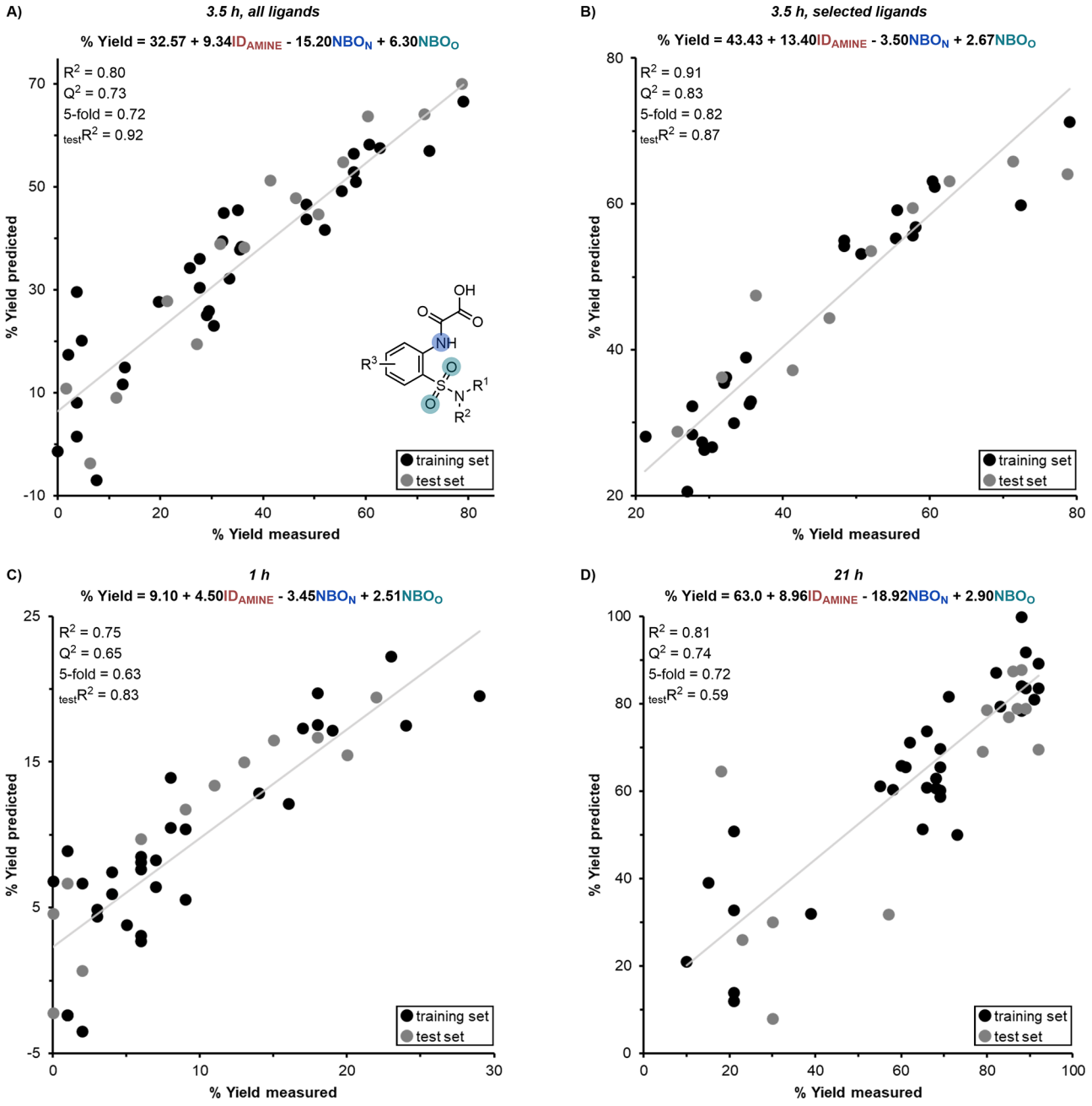

Figure 3. (A) Linear model describing the impact of ligand on the reaction yield at 3.5 h. Full ligand set included. (B) Linear model using the same descriptors in the truncated ligand set. Data modeled at 3.5 h are the average of three runs. Two NBO descriptors dictate reactivity throughout the course of the reaction. Linear models for the full data set are also shown for yield at 1 h (C) and 21 h (D).

To further explore the interplay of these two parameters on reactivity, a scatter plot of NBO(O) vs NBO(N) colored by average % yield was constructed (Figure 4A). This visualization depicts the range of ligand NBO values optimal for this coupling (upper left quadrant). In tandem with the presented linear models, this plot provides a platform to help guide future ligand design and balance desired electronic features of the ligand. As illustrated by **L5** and **L22**, increasing the magnitude of NBO(N) and decreasing the magnitude of NBO(O) improves the reaction yield; however, modulating a specific structural feature of the ligand often impacts both values. Thus, it is challenging to design a ligand capable of achieving both the optimal NBO charges simultaneously [e.g., NBO(N) of −0.60 and NBO(O) of −0.88]. Instead, ligands can be selected to optimize one feature or, ideally, to strike a balance between the two descriptors (e.g., the high yielding ligands that fall between **L5** and **L22** in the plot).

We next sought to use a combination of models to design ligands with improved reactivity. We thus designed a set of untested ligands with varied structures at the sulfonamide amine and phenylene backbone in an effort to vary the electronic profile of the ligands. These virtual ligands were subjected to the same computational workflow as the training ligands, and their NBO(O) and NBO(N) partial charge values were used to predict the cross-coupling yield of each

https://doi.org/10.1021/acscatal.3c04566
ACS Catal. 2023, 13, 16195−16206

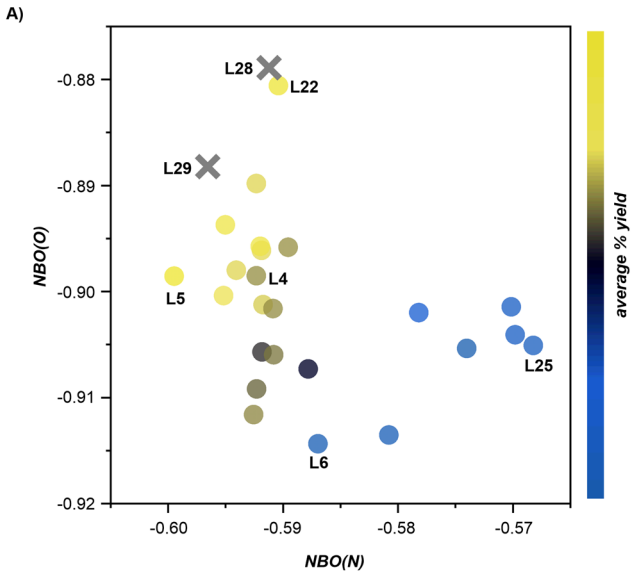

B)

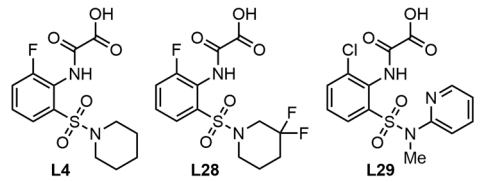

Catalyst/L Loading	Amine	L4	L28	L29
		Yield		
30 mol%	**2b**	42%	49%	60%
	2c	24%	24%	31%
10 mol%	**2b**	20%	23%	36%
	2c	12%	15%	24%

Figure 4. (A) Descriptors identified through linear modeling can also be used to visualize the active ligand space. Points are colored according to average % yield for the two substrates at 3.5 h, where blue corresponds to low yield and yellow corresponds to high yield. Two new ligands were designed to access the new chemical space (gray Xs, **L28** and **L29**). (B) These ligands were tested along with **L4** using the conditions in Figure 2 and with a lower catalyst/ligand loading.

amine at each time point. Several ligand structures were consistently predicted to perform well with each variation of our statistical models (full ligand set and selected ligand set at 1, 3.5, and 21 h). These virtual ligands (**L28**, **L29**, Figure 4B) were visualized on the chemical space map (Figure 4A).

Based on the linear model predictions and this visualization, we selected ligands **L28** and **L29** to synthesize and test in the cross-couplings with amines **2b** and **2c**, with aryl bromide **1a**, under optimized conditions (Figure 2). While **L28** possesses NBO(O) and NBO(N) values similar to those of **L22**, **L29** notably occupies a chemical space not achieved by our training ligands. Both of these ligands performed as well or better than our lead ligand (**L4**) for coupling of each amine (Figure 4B). These ligands were then challenged by reducing the catalyst loading to 10 mol %. At the lower loading, use of ligand **L28** led to a modest improvement in yield (compared to **L4**), but ligand **L29** imparted an approximately 2-fold increase in yield for these amines. The results highlight the advantage of targeting a chemical space that balances both NBO descriptors and demonstrate that our model can be used to predict new ligand structures that can promote the reaction with higher efficiency.

For the scope evaluation presented below, we opted to use **L4** as it was commercially available (Millipore Sigma, product #805491) and exhibited reasonable reactivity with multiple classes of α-branched amine nucleophiles (**2a**, **2b**, and **2c**). We note that **L4** was not the most effective ligand for the coupling of amines **2b** and **2c** with halide **1a**, but it was a strong performer with a relatively balanced NBO(O) and NBO(N) profile.

Evaluation of Substrate Scope. Having optimized the reaction conditions and explored the effect of ligand structure, we next focused on evaluating the substrate scope (Table 3). In terms of the amine coupling partner, secondary cyclic 5- and 6- membered α-branched amines reacted efficiently (**3b**−**3e**). Examples **3c** and **3d** demonstrate that an alkyl ether or alkyl amine bound to the α-branched amine is well tolerated. Secondary and primary acyclic α-branched amines reacted in modest to high yields (**3f**−**3i**), and 2-aryl-pyrrolidines reacted well (**3j**−**3n**). Lastly, secondary bicyclic branched amines coupled efficiently (**3o**−**3u**). In terms of the aryl bromide scope, electron-poor and electron-rich aryl halides reacted efficiently with various amine partners, and Table 3 presents coupling examples of a series of desirable heterocyclic aryl halides such as those based on pyridine (**3e**, **3k**), pyridone (**3t**), thiazole (**3d**, **3h**, **3i**, **3s**), pyrazole (**3o**, **3p**), imidazole (**3r**), and tetrazole (**3u**). These classes of nitrogen-containing heterocycles are some of the most commonly encountered in pharmaceuticals,[84] and aside from a recent elegant report from the Buchwald lab,[34] they are only sparsely demonstrated in other methods focused on cross-coupling of α-branched amines.

Encouraged by our initial scope exploration, we set out to assess the C−N coupling performance in the context of druglike substrates (Figure 5). We first tested α-branched amines **2d** and **2e** against the entire set of informer aryl halides[35] in a miniaturized parallel high-throughput synthesis experiment (Figure 5A). The informer aryl halides are useful substrates to measure the effectiveness of a synthetic method as these structures were intermediates in drug discovery campaigns and sample druglike chemical space. Additionally, the informer aryl halides have been tested against other C−N coupling conditions with simple amine substrates, providing a useful benchmark for newly developed methods.[85] Reactions were conducted on 0.015 mmol scale in a miniaturized HTE well plate format with 60 mol % Cu_2O/**L4**[63] and monitored by UPLC/MS. Reaction products and byproducts were assigned by ESI mass spectrometry, and reaction conversion was computed using UV 210 nm peak areas.[63] For practical medicinal chemistry purposes, a reaction conversion ≥20% typically provides enough product after purification for biological testing. Setting this as a threshold and applying our optimized method, we were able to observe >20% conversion to the desired product in 8 out of 18 informers (**X1**−**4**, **X6**, **X8**, **X14**, and **X15**) using amine **2d** and 6 of 18 informers (**X1**−**3**, **X6**, **X13**, and **X15**) using amine **2e**. There remain gaps in the set of informers that react productively, namely, **X7**, **X9**−**12**, **X16**−**18** provide little to no observable product in this experiment. This is similar to the results observed in the original informer study using **L4** and piperidine.[35,86]

We next focused on cross-coupling informer aryl halides on a larger scale with various amine nucleophiles (including **2d**

https://doi.org/10.1021/acscatal.3c04566
ACS Catal. 2023, 13, 16195−16206

Table 3. Initial Exploration of the Substrate Scope[a]

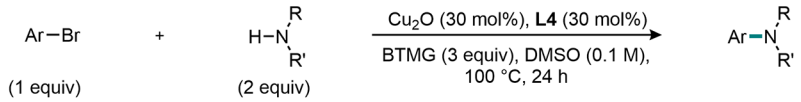

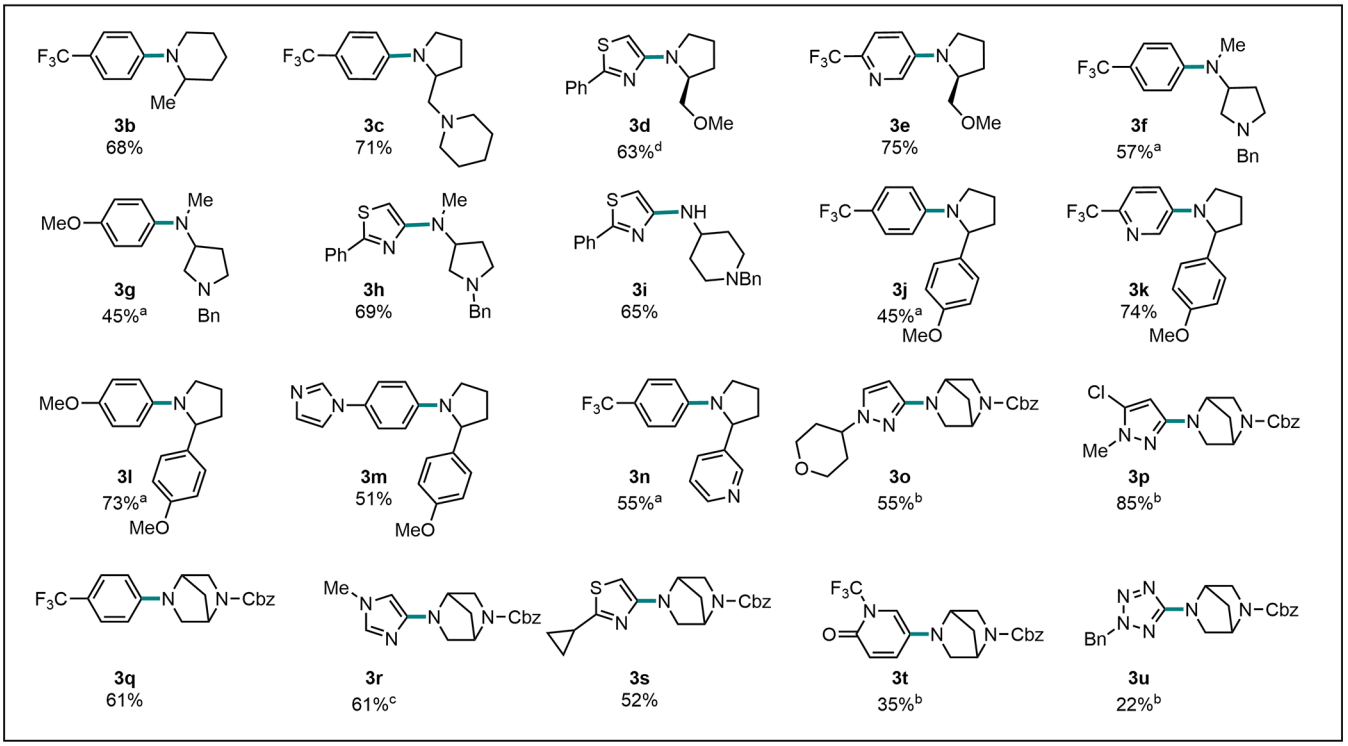

[a]Reactions performed on 0.15 mmol scale unless noted. [b]0.5 mmol scale. [c]0.2 mmol scale. [d]*N*-Me-3-Iodo-imidazole was used. [e]60 mol % **L4** and Cu_2O was used.

and **2e**) that were observed to have relatively high conversion in the miniaturized parallel high-throughput experiment. Informer **X2** was successfully cross-coupled with amine **2d** to form **3v** in 80% yield, 2-Me-piperidine to form **3a** in 53% yield (from Table 1), and 2-Et-piperidine to form **3w** in 45% yield. Modest reactivity with 2-Et-piperpidine is notable as few methods that promote α-branched amine and aryl halide cross-coupling are compatible with this type of hindered amine nucleophile.[31,33] Informer **X3** reacted in moderate to good yield with a series of amines including **2d** and **2e** to form **3x** and **3y** in 62 and 60% yields, respectively, and an α-amino-alcohol to form **3z** in 75% yield. In the case of product **3z**, when 0 equiv of **L4** was added, no conversion occurred.[63] Informer **X3** also reacted cleanly with bicyclic secondary amines to form products like **3aa** (78% yield). Informer **X6** reacted with **2e** to form **3ab** in 52% yield and *N*-Me-*N*-cyclohexyl amine to form product **3ac** in 73% yield. However, a steep reactivity cliff was observed when attempting to couple **X6** with the *N*-Et-*N*-cyclohexyl amine to form **3ad**. The reaction proceeded in 0% yield with no observable conversion of **X6** taking place.[63] Informer **X15** reacted with **2d** to form **3ae** in 49% yield and *N*-Me-*N*-cyclohexyl amine to form **3af** in 53% yield. The reaction performance for **3v**, **3x**, **3y**, **3ab**, and **3ae** was measured both in the miniaturized HTE format (Figure 5A) and on a larger scale, demonstrating how the miniaturized HTE results translate to reactions performed on larger scale.[87] Encouraged by these results, we also attempted the late-stage arylation of a complex α-branched primary amine, the pharmaceutical agent sitagliptin (**2f**) (Figure 5C). We observed productive coupling with a variety of aryl halides **1b−1d,** which include an alcohol, chloropyrazole, and pyridine substructure. These results also demonstrated translation of the reaction conditions to a case where a complex amine is employed as the limiting reagent. Overall, the data presented in Figure 5 demonstrate that the process tolerates a wide range of functional groups and complex structures found in pharmaceutical compounds and that the method is applicable in modern miniaturized parallel HTE.

Our next goal was to demonstrate a parallel medicinal library synthesis through the late-stage amination of trametinib (Figure 6). We selected α-branched amines that might be reactive based on our previous work and evaluated their coupling with trametinib (**1f**) using our optimized conditions. These reactions were executed in a miniaturized parallel HTE reactor, and we monitored the reactions by UPLC/MS using MS to assign the peaks. The heat map in Figure 6 is colored by product conversion using the UV254 nm signal.[63] A broad range of amines were observed to react with trametinib in synthetically useful conversions, including secondary and primary α-branched amines and bicyclic amines. In all, 22 of 24 reactions proceeded in ≥20% conversion, and we selected 9 cases for purification, quantitative yield measurement, and characterization, the results of which are shown in Figure 6.[63]

https://doi.org/10.1021/acscatal.3c04566
ACS Catal. 2023, 13, 16195−16206

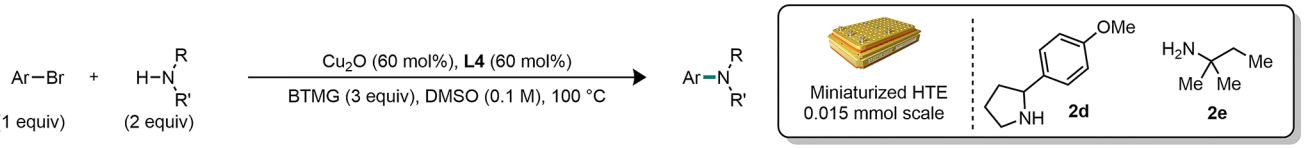

A) Conversion data for all informer aryl halides (**X1-X18**) coupled with **2d** and **2e**

Low % conv. High

Amine	X1	X2	X3	X4	X5	X6	X7	X8	X9	X10	X11	X12	X13	X14	X15	X16	X17	X18
2d	43	83	84	64	18	78	0	29	0	4	0	11	1	43	80	0	0	14
2e	34	52	63	12	4	68	0	10	0	5	0	7	38	0	72	0	0	13

B) C-N coupling of informer aryl bromides with various amines

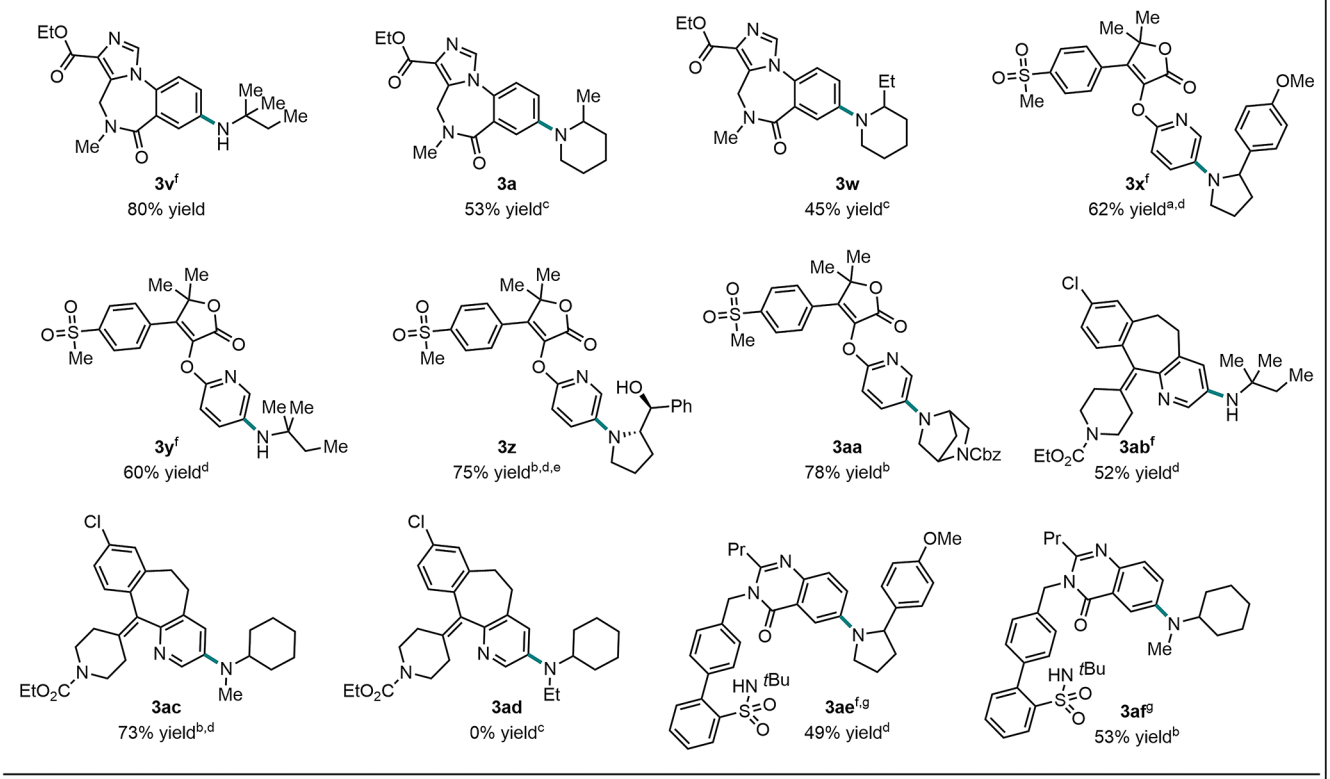

C) Arylation of sitigliptin

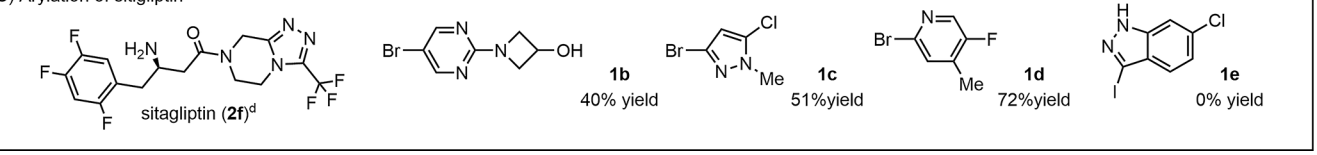

Figure 5. (A) Conversion data for all informer aryl halides coupled with **2d** and **2e**. Reactions were executed on 0.015 mmol scale in a miniaturized HTE reactor, and reaction performance is reported as % conversion based on peak areas at 215 nm.[63] See supplemental for informer aryl halide structures. (B) Informer aryl halide coupling performed on 0.3 mmol scale unless noted, [a]0.6 mmol scale, [b] 0.2 mmol scale, [c]0.1 mmol scale, [d]30 mol % **L4** and Cu_2O were used, [e]0% **L4**, 0% yield, [f]experiment included in small scale set (Figure 5A), and [g] ArI was used instead of ArBr. (C) Late-stage modification of sitagliptin performed on 0.3 mmol scale. 1 equiv sitagliptin (**2f**); 2 equiv aryl halide.

CONCLUSIONS

We developed a new method for the synthesis of αBAAs by cross-coupling aryl halides and α-branched amines as building blocks. The reaction is operationally simple to execute, is broad in scope, and can be used to deliver medicinal analogues using complex aryl halides and amines. The chemistry is HTE-enabled, allowing for direct translation of plate-based miniaturized reaction optimization to medicinal analogue synthesis in parallel. We also interrogated the ligand structure using HTE and have developed a statistical model that helps us to better understand the features of the ligands in this class [NBO(O) and NBO (N)]. Our intent was to develop a method applicable in medicinal chemistry (generality and broad scope),[88] but we note that our ligand SAR study and statistical models provide a platform for informed ligand design that might lead to more efficient catalytic systems.[89]

https://doi.org/10.1021/acscatal.3c04566
ACS Catal. 2023, 13, 16195−16206

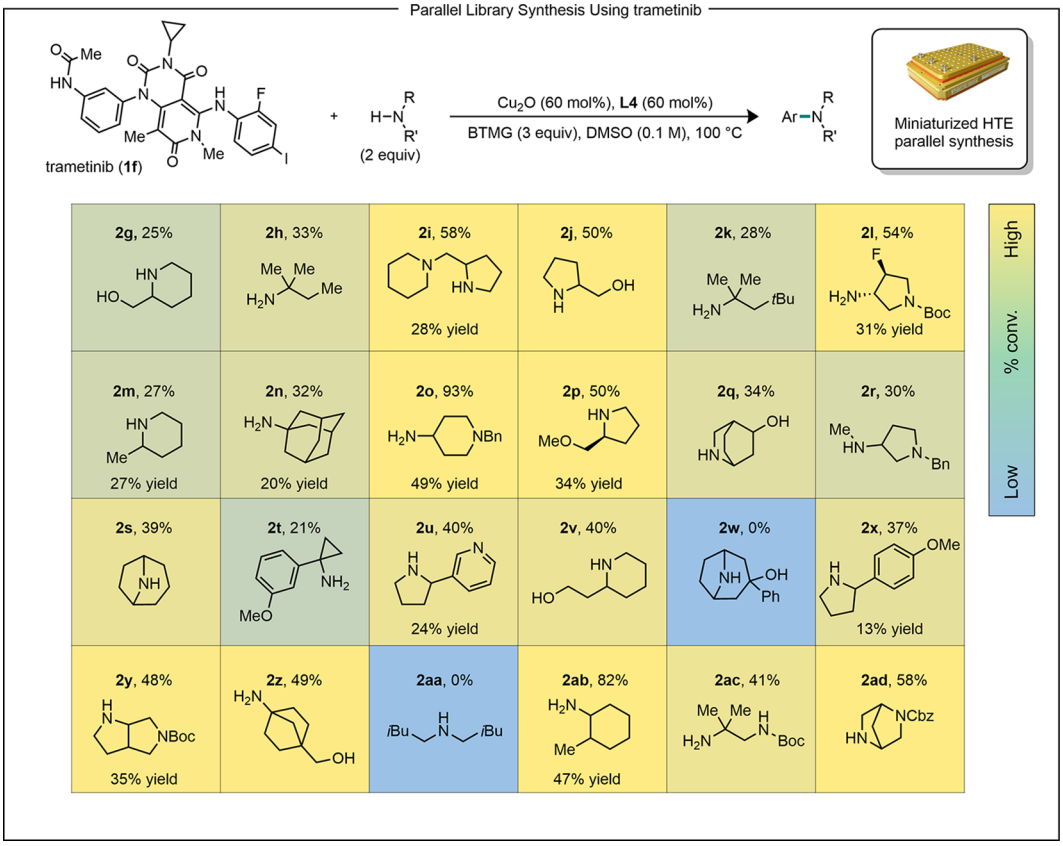

Figure 6. Parallel library synthesis of trametinib (**1f**), 9 mg scale (25 μmol). The % conversion is presented above the amines in the heat map, and the heat map is colored by conversion. If the product was isolated and characterized, the yield is given below the amine structure.

■ ASSOCIATED CONTENT

Supporting Information

The Supporting Information is available free of charge at https://pubs.acs.org/doi/10.1021/acscatal.3c04566.

Descriptors (XLSX)

Cartesian coordinates (PDF)

Characterization data for all new compounds, general procedures, HTE data and other data (PDF)

■ AUTHOR INFORMATION

Corresponding Authors

Matthew S. Sigman − *Department of Chemistry, University of Utah, Salt Lake City, Utah 84112, United States;* orcid.org/0000-0002-5746-8830; Email: matt.sigman@utah.edu

Mycah R. Uehling − *Merck & Co., Inc., Rahway, New Jersey 07033, United States;* orcid.org/0000-0002-5281-1935; Email: mycah.uehling@merck.com

Authors

Adrian D. Matthews − *Merck & Co., Inc., Rahway, New Jersey 07033, United States;* orcid.org/0000-0003-4320-4057

Ellyn Peters − *Department of Chemistry, University of Utah, Salt Lake City, Utah 84112, United States*

John S. Debenham − *Merck & Co., Inc., Rahway, New Jersey 07033, United States;* orcid.org/0000-0002-9327-2835

Qi Gao − *Merck & Co., Inc., Rahway, New Jersey 07033, United States;* orcid.org/0000-0001-5425-2471

Maya D. Nyamiaka − *Merck & Co., Inc., Rahway, New Jersey 07033, United States*

Jianping Pan − *Merck & Co., Inc., Rahway, New Jersey 07033, United States*

Li-Kang Zhang − *Merck & Co., Inc., Rahway, New Jersey 07033, United States;* orcid.org/0000-0003-3757-8116

Spencer D. Dreher − *Merck & Co., Inc., Rahway, New Jersey 07033, United States;* orcid.org/0000-0002-5094-1218

Shane W. Krska − *Merck & Co., Inc., Rahway, New Jersey 07033, United States;* orcid.org/0000-0001-9757-9036

Complete contact information is available at: https://pubs.acs.org/10.1021/acscatal.3c04566

Author Contributions

[§]A.D.M. and E.P. contributed equally. The manuscript was written through contributions of all authors and all authors have given approval to the final version of the manuscript.

Notes

The authors declare no competing financial interest.

■ ACKNOWLEDGMENTS

M.S.S. and E.P. acknowledge the financial support from the NSF under the CCI Center for Computer Assisted Synthesis (CHE-1925607 and CHE-2202693) and acknowledge Dr. Cian Kingston for helpful discussions. The support and resources from the Center for High Performance Computing

at the University of Utah are gratefully acknowledged. A.D.M. acknowledges the Future Talent Program at Merck & Co., Inc., Rahway, NJ, USA for support during a Co-op in Discovery Chemistry. M.R.U. acknowledges helpful discussions with Dr. Dipannita Kalyani, Dr. Dane Clausen, and Dr. Yuriy Slutskyy. We acknowledge Na Meng and Dr. Ramu Rondla for assistance with ligand synthesis.

■ ABBREVIATIONS

HTE, high-throughput experimentation

■ REFERENCES

(1) Cushing, T. D.; Hao, X.; Shin, Y.; Andrews, K.; Brown, M.; Cardozo, M.; Chen, Y.; Duquette, J.; Fisher, B.; Gonzalez-Lopez de Turiso, F.; He, X.; Henne, K. R.; Hu, Y.-L.; Hungate, R.; Johnson, M. G.; Kelly, R. C.; Lucas, B.; McCarter, J. D.; McGee, L. R.; Medina, J. C.; San Miguel, T.; Mohn, D.; Pattaropong, V.; Pettus, L. H.; Reichelt, A.; Rzasa, R. M.; Seganish, J.; Tasker, A. S.; Wahl, R. C.; Wannberg, S.; Whittington, D. A.; Whoriskey, J.; Yu, G.; Zalameda, L.; Zhang, D.; Metz, D. P. Discovery and in Vivo Evaluation of (S)-N-(1-(7-Fluoro-2-(pyridin-2-yl)quinolin-3-yl)-ethyl)-9H-purin-6-amine (AMG319) and Related PI3Kδ Inhibitors for Inflammation and Autoimmune Disease. *J. Med. Chem.* **2015**, *58* (1), 480−511.

(2) Pasquier, B.; El-Ahmad, Y.; Filoche-Rommé, B.; Dureuil, C.; Fassy, F.; Abecassis, P.-Y.; Mathieu, M.; Bertrand, T.; Benard, T.; Barrière, C.; El Batti, S.; Letallec, J.-P.; Sonnefraud, V.; Brollo, M.; Delbarre, L.; Loyau, V.; Pilorge, F.; Bertin, L.; Richepin, P.; Arigon, J.; Labrosse, J.-R.; Clément, J.; Durand, F.; Combet, R.; Perraut, P.; Leroy, V.; Gay, F.; Lefrançois, D.; Bretin, F.; Marquette, J.-P.; Michot, N.; Caron, A.; Castell, C.; Schio, L.; McCort, G.; Goulaouic, H.; Garcia-Echeverria, C.; Ronan, B. Discovery of (2S)-8-[(3R)-3-Methylmorpholin-4-yl]-1-(3-methyl-2-oxobutyl)-2-(trifluoromethyl)-3,4-dihydro-2H-pyrimido[1,2-a]pyrimidin-6-one: A Novel Potent and Selective Inhibitor of Vps34 for the Treatment of Solid Tumors. *J. Med. Chem.* **2015**, *58* (1), 376−400.

(3) Lovering, F.; Bikker, J.; Humblet, C. Escape from Flatland: Increasing Saturation as an Approach to Improving Clinical Success. *J. Med. Chem.* **2009**, *52* (21), 6752−6756.

(4) Degorce, S. L.; Bodnarchuk, M. S.; Cumming, I. A.; Scott, J. S. Lowering Lipophilicity by Adding Carbon: One-Carbon Bridges of Morpholines and Piperazines. *J. Med. Chem.* **2018**, *61* (19), 8934−8943.

(5) Pike, K. G.; Malagu, K.; Hummersone, M. G.; Menear, K. A.; Duggan, H. M. E.; Gomez, S.; Martin, N. M. B.; Ruston, L.; Pass, S. L.; Pass, M. Optimization of potent and selective dual mTORC1 and mTORC2 inhibitors: The discovery of AZD8055 and AZD2014. *Bioorgan. Med. Chem. Lett.* **2013**, *23* (5), 1212−1216.

(6) Larsen, M. A.; Hennessy, E. T.; Deem, M. C.; Lam, Y.-h.; Saurí, J.; Sather, A. C. A Modular and Diastereoselective 5 + 1 Cyclization Approach to N-(Hetero)Aryl Piperidines. *J. Am. Chem. Soc.* **2020**, *142* (2), 726−732.

(7) Ichikawa, S.; Zhu, S.; Buchwald, S. L. A Modified System for the Synthesis of Enantioenriched N-Arylamines through Copper-Catalyzed Hydroamination. *Angew. Chem., Int. Ed.* **2018**, *57* (28), 8714−8718.

(8) Fisher, D. J.; Shaum, J. B.; Mills, C. L.; Read de Alaniz, J. Synthesis of Hindered Anilines: Three-Component Coupling of Arylboronic Acids, tert-Butyl Nitrite, and Alkyl Bromides. *Org. Lett.* **2016**, *18* (19), 5074−5077.

(9) Mailig, M.; Rucker, R. P.; Lalic, G. Practical catalytic method for synthesis of sterically hindered anilines. *Chem. Commun.* **2015**, *51* (55), 11048−11051.

(10) Gui, J.; Pan, C.-M.; Jin, Y.; Qin, T.; Lo, J. C.; Lee, B. J.; Spergel, S. H.; Mertzman, M. E.; Pitts, W. J.; Cruz, T. E. L.; Schmidt, M. A.; Darvatkar, N.; Natarajan, S. R.; Baran, P. S. Practical olefin hydroamination with nitroarenes. *Science* **2015**, *348* (6237), 886−891.

(11) Rucker, R. P.; Whittaker, A. M.; Dang, H.; Lalic, G. Synthesis of Hindered Anilines: Copper-Catalyzed Electrophilic Amination of Aryl Boronic Esters. *Angew. Chem., Int. Ed.* **2012**, *51* (16), 3953−3956.

(12) Ye, W.-T.; Zhu, R. Dioxygen-promoted cobalt-catalyzed oxidative hydroamination using unactivated alkenes and free amines. *Chem. Catalysis* **2022**, *2* (2), 345−357.

(13) Dighe, U. S.; Juliá, F.; Luridiana, A.; Douglas, J. J.; Leonori, D. A photochemical dehydrogenative strategy for aniline synthesis. *Nature* **2020**, *584* (7819), 75−81.

(14) Greenwood, J. W.; Larsen, M. A.; Burgess, S. A.; Newman, J. A.; Jiang, Y.; Sather, A. C. Isolable iminium ions as a platform for N-(hetero)aryl piperidine synthesis. *Nature Synthesis* **2023**, *2* (11), 1059−1067.

(15) Wang, Y.; Haight, I.; Gupta, R.; Vasudevan, A. What is in Our Kit? An Analysis of Building Blocks Used in Medicinal Chemistry Parallel Libraries. *J. Med. Chem.* **2021**, *64* (23), 17115−17122.

(16) Ruiz-Castillo, P.; Buchwald, S. L. Applications of Palladium-Catalyzed C−N Cross-Coupling Reactions. *Chem. Rev.* **2016**, *116* (19), 12564−12649.

(17) Bhunia, S.; Pawar, G. G.; Kumar, S. V.; Jiang, Y.; Ma, D. Selected Copper-Based Reactions for C−N, C−O, C−S, and C−C Bond Formation. *Angew. Chem., Int. Ed.* **2017**, *56* (51), 16136−16179.

(18) Hartwig, J. F. Evolution of a Fourth Generation Catalyst for the Amination and Thioetherification of Aryl Halides. *Acc. Chem. Res.* **2008**, *41* (11), 1534−1544.

(19) Ingoglia, B. T.; Wagen, C. C.; Buchwald, S. L. Biaryl monophosphine ligands in palladium-catalyzed C−N coupling: An updated User's guide. *Tetrahedron* **2019**, *75* (32), 4199−4211.

(20) Li, C.; Kawamata, Y.; Nakamura, H.; Vantourout, J. C.; Liu, Z.; Hou, Q.; Bao, D.; Starr, J. T.; Chen, J.; Yan, M.; Baran, P. S. Electrochemically Enabled, Nickel-Catalyzed Amination. *Angew. Chem., Int. Ed.* **2017**, *56* (42), 13088−13093.

(21) Iwai, T.; Harada, T.; Shimada, H.; Asano, K.; Sawamura, M. A Polystyrene-Cross-Linking Bisphosphine: Controlled Metal Monochelation and Ligand-Enabled First-Row Transition Metal Catalysis. *ACS Catal.* **2017**, *7* (3), 1681−1692.

(22) Corcoran, E. B.; Pirnot, M. T.; Lin, S.; Dreher, S. D.; DiRocco, D. A.; Davies, I. W.; Buchwald, S. L.; MacMillan, D. W. C. Aryl amination using ligand-free Ni(II) salts and photoredox catalysis. *Science* **2016**, *353* (6296), 279−283.

(23) Li, D.-H.; Lan, X.-B.; Song, A.-X.; Rahman, M. M.; Xu, C.; Huang, F.-D.; Szostak, R.; Szostak, M.; Liu, F.-S. Buchwald-Hartwig Amination of Coordinating Heterocycles Enabled by Large-but-Flexible Pd-BIAN-NHC Catalysts**. *Chem. − Eur. J.* **2022**, *28* (4), No. e202103341.

(24) Bigler, R.; Spiess, D.; Wellauer, J.; Binder, M.; Carré, V.; Fantasia, S. Synthesis of Biaryl Phosphine Palladium(0) Precatalysts. *Organometallics* **2021**, *40* (15), 2384−2388.

(25) Tassone, J. P.; England, E. V.; MacQueen, P. M.; Ferguson, M. J.; Stradiotto, M. PhPAd-DalPhos: Ligand-Enabled, Nickel-Catalyzed Cross-Coupling of (Hetero)aryl Electrophiles with Bulky Primary Alkylamines. *Angew. Chem., Int. Ed.* **2019**, *58* (8), 2485−2489.

(26) Ruiz-Castillo, P.; Blackmond, D. G.; Buchwald, S. L. Rational Ligand Design for the Arylation of Hindered Primary Amines Guided by Reaction Progress Kinetic Analysis. *J. Am. Chem. Soc.* **2015**, *137* (8), 3085−3092.

(27) Zhang, Y.; Lavigne, G.; Lugan, N.; César, V. Buttressing Effect as a Key Design Principle towards Highly Efficient Palladium/N-Heterocyclic Carbene Buchwald−Hartwig Amination Catalysts. *Chem. − Eur. J.* **2017**, *23* (55), 13792−13801.

(28) Tassone, J. P.; Lundrigan, T.; Ashton, T. D.; Stradiotto, M. Nickel-Catalyzed C−N Cross-Coupling of 4-Chloro-1,8-naphthalimides and Bulky, Primary Alkylamines at Room Temperature. *J. Org. Chem.* **2022**, *87* (9), 6492−6498.

(29) Wang, Z.-C.; Li, Y.-Y.; Zhang, S.-Q.; Hong, X.; Shi, S.-L. Unsymmetric N-heterocyclic carbene ligand enabled nickel-catalysed

https://doi.org/10.1021/acscatal.3c04566
ACS Catal. 2023, 13, 16195−16206

arylation of bulky primary and secondary amines. *Chem. Sci.* **2023**, *14* (16), 4390−4396.
(30) Khadra, A.; Mayer, S.; Mitchell, D.; Rodriguez, M. J.; Organ, M. G. A General Protocol for the Broad-Spectrum Cross-Coupling of Nonactivated Sterically Hindered 1° and 2° Amines. *Organometallics* **2017**, *36* (18), 3573−3577.
(31) Park, N. H.; Vinogradova, E. V.; Surry, D. S.; Buchwald, S. L. Design of New Ligands for the Palladium-Catalyzed Arylation of α-Branched Secondary Amines. *Angew. Chem., Int. Ed.* **2015**, *54* (28), 8259−8262.
(32) Nett, A. J.; Cañellas, S.; Higuchi, Y.; Robo, M. T.; Kochkodan, J. M.; Haynes, M. T.; Kampf, J. W.; Montgomery, J. Stable, Well-Defined Nickel(0) Catalysts for Catalytic C−C and C−N Bond Formation. *ACS Catal.* **2018**, *8* (7), 6606−6611.
(33) Wang, Z.-C.; Xie, P.-P.; Xu, Y.; Hong, X.; Shi, S.-L. Low-Temperature Nickel-Catalyzed C−N Cross-Coupling via Kinetic Resolution Enabled by a Bulky and Flexible Chiral N-Heterocyclic Carbene Ligand. *Angew. Chem., Int. Ed.* **2021**, *60* (29), 16077−16084.
(34) Reichert, E. C.; Feng, K.; Sather, A. C.; Buchwald, S. L. Pd-Catalyzed Amination of Base-Sensitive Five-Membered Heteroaryl Halides with Aliphatic Amines. *J. Am. Chem. Soc.* **2023**, *145* (6), 3323−3329.
(35) Kutchukian, P. S.; Dropinski, J. F.; Dykstra, K. D.; Li, B.; DiRocco, D. A.; Streckfuss, E. C.; Campeau, L.-C.; Cernak, T.; Vachal, P.; Davies, I. W.; Krska, S. W.; Dreher, S. D. Chemistry informer libraries: a chemoinformatics enabled approach to evaluate and advance synthetic methods. *Chem. Sci.* **2016**, *7* (4), 2604−2613.
(36) Modak, A.; Nett, A. J.; Swift, E. C.; Haibach, M. C.; Chan, V. S.; Franczyk, T. S.; Shekhar, S.; Cook, S. P. Cu-Catalyzed C−N Coupling with Sterically Hindered Partners. *ACS Catal.* **2020**, *10* (18), 10495−10499.
(37) de Gombert, A.; Darù, A.; Ahmed, T. S.; Haibach, M. C.; Li-Matsuura, R.; Yang, C.; Henry, R. F.; Cook, S. P.; Shekhar, S.; Blackmond, D. G. Mechanistic Insight into Cu-Catalyzed C−N Coupling of Hindered Aryl Iodides and Anilines Using a Pyrrol-ol Ligand Enables Development of Mild and Homogeneous Reaction Conditions. *ACS Catal.* **2023**, *13* (5), 2904−2915.
(38) Kim, S.-T.; Strauss, M. J.; Cabré, A.; Buchwald, S. L. Room-Temperature Cu-Catalyzed Amination of Aryl Bromides Enabled by DFT-Guided Ligand Design. *J. Am. Chem. Soc.* **2023**, *145* (12), 6966−6975.
(39) Gao, J.; Bhunia, S.; Wang, K.; Gan, L.; Xia, S.; Ma, D. Discovery of N-(Naphthalen-1-yl)-N′-alkyl Oxalamide Ligands Enables Cu-Catalyzed Aryl Amination with High Turnovers. *Org. Lett.* **2017**, *19* (11), 2809−2812.
(40) Ding, X.; Huang, M.; Yi, Z.; Du, D.; Zhu, X.; Wan, Y. Room-Temperature CuI-Catalyzed Amination of Aryl Iodides and Aryl Bromides. *J. Org. Chem.* **2017**, *82* (10), 5416−5423.
(41) Bhunia, S.; Kumar, S. V.; Ma, D. N,N′-Bisoxalamides Enhance the Catalytic Activity in Cu-Catalyzed Coupling of (Hetero)Aryl Bromides with Anilines and Secondary Amines. *J. Org. Chem.* **2017**, *82* (23), 12603−12612.
(42) Zhang, Y.; Yang, X.; Yao, Q.; Ma, D. CuI/DMPAO-Catalyzed N-Arylation of Acyclic Secondary Amines. *Org. Lett.* **2012**, *14* (12), 3056−3059.
(43) Mennen, S. M.; Alhambra, C.; Allen, C. L.; Barberis, M.; Berritt, S.; Brandt, T. A.; Campbell, A. D.; Castañón, J.; Cherney, A. H.; Christensen, M.; Damon, D. B.; Eugenio de Diego, J.; García-Cerrada, S.; García-Losada, P.; Haro, R.; Janey, J.; Leitch, D. C.; Li, L.; Liu, F.; Lobben, P. C.; MacMillan, D. W. C.; Magano, J.; McInturff, E.; Monfette, S.; Post, R. J.; Schultz, D.; Sitter, B. J.; Stevens, J. M.; Strambeanu, I. I.; Twilton, J.; Wang, K.; Zajac, M. A. The Evolution of High-Throughput Experimentation in Pharmaceutical Development and Perspectives on the Future. *Org. Process Res. Dev.* **2019**, *23* (6), 1213−1242.
(44) Shevlin, M. Practical High-Throughput Experimentation for Chemists. *ACS Med. Chem. Lett.* **2017**, *8* (6), 601−607.
(45) Krska, S. W.; DiRocco, D. A.; Dreher, S. D.; Shevlin, M. The Evolution of Chemical High-Throughput Experimentation To Address Challenging Problems in Pharmaceutical Synthesis. *Acc. Chem. Res.* **2017**, *50* (12), 2976−2985.
(46) Cernak, T.; Gesmundo, N. J.; Dykstra, K.; Yu, Y.; Wu, Z.; Shi, Z.-C.; Vachal, P.; Sperbeck, D.; He, S.; Murphy, B. A.; Sonatore, L.; Williams, S.; Madeira, M.; Verras, A.; Reiter, M.; Lee, C. H.; Cuff, J.; Sherer, E. C.; Kuethe, J.; Goble, S.; Perrotto, N.; Pinto, S.; Shen, D.-M.; Nargund, R.; Balkovec, J.; DeVita, R. J.; Dreher, S. D. Microscale High-Throughput Experimentation as an Enabling Technology in Drug Discovery: Application in the Discovery of (Piperidinyl)pyridinyl-1H-benzimidazole Diacylglycerol Acyltransferase 1 Inhibitors. *J. Med. Chem.* **2017**, *60* (9), 3594−3605.
(47) Dykstra, K. D.; Streckfuss, E.; Liu, M.; Liu, J.; Yu, Y.; Wang, M.; Kozlowski, J. A.; Myers, R. W.; Buevich, A. V.; Maletic, M. M.; Vachal, P.; Krska, S. W. Synthesis of HDAC Inhibitor Libraries via Microscale Workflow. *ACS Med. Chem. Lett.* **2021**, *12* (3), 337−342.
(48) Barhate, C. L.; Donnell, A. F.; Davies, M.; Li, L.; Zhang, Y.; Yang, F.; Black, R.; Zipp, G.; Zhang, Y.; Cavallaro, C. L.; Priestley, E. S.; Weller, H. N. Microscale purification in support of high-throughput medicinal chemistry. *Chem. Commun.* **2021**, *57* (84), 11037−11040.
(49) Hettiarachchi, K.; Hayes, M.; Desai, A. J.; Wang, J.; Ren, Z.; Greshock, T. J. Subminute micro-isolation of pharmaceuticals with ultra-high pressure liquid chromatography. *J. Pharmaceut. and Biomed.* **2019**, *176*, No. 112794.
(50) Hettiarachchi, K.; Streckfuss, E.; Sanzone, J. R.; Wang, J.; Hayes, M.; Kong, M.; Greshock, T. J. Microscale Purification with Direct Charged Aerosol Detector Quantitation Using Selective Online One- or Two-Dimensional Liquid Chromatography. *Anal. Chem.* **2022**, *94* (23), 8309−8316.
(51) Santanilla, A. B.; Regalado, E. L.; Pereira, T.; Shevlin, M.; Bateman, K.; Campeau, L.-C.; Schneeweis, J.; Berritt, S.; Shi, Z.-C.; Nantermet, P.; Liu, Y.; Helmy, R.; Welch, C. J.; Vachal, P.; Davies, I. W.; Cernak, T.; Dreher, S. D. Nanomole-scale high-throughput chemistry for the synthesis of complex molecules. *Science* **2015**, *347* (6217), 49−53.
(52) Gao, K.; Shaabani, S.; Xu, R.; Zarganes-Tzitzikas, T.; Gao, L.; Ahmadianmoghaddam, M.; Groves, M. R.; Dömling, A. Nanoscale, automated, high throughput synthesis and screening for the accelerated discovery of protein modifiers. *RSC Med. Chem.* **2021**, *12* (5), 809−818.
(53) Gesmundo, N. J.; Sauvagnat, B.; Curran, P. J.; Richards, M. P.; Andrews, C. L.; Dandliker, P. J.; Cernak, T. Nanoscale synthesis and affinity ranking. *Nature* **2018**, *557* (7704), 228−232.
(54) Thomas, R. P.; Heap, R. E.; Zappacosta, F.; Grant, E. K.; Pogány, P.; Besley, S.; Fallon, D. J.; Hann, M. M.; House, D.; Tomkinson, N. C. O.; Bush, J. T. A direct-to-biology high-throughput chemistry approach to reactive fragment screening. *Chem. Sci.* **2021**, *12* (36), 12098−12106.
(55) Hendrick, C. E.; Jorgensen, J. R.; Chaudhry, C.; Strambeanu, I. I.; Brazeau, J.-F.; Schiffer, J.; Shi, Z.; Venable, J. D.; Wolkenberg, S. E. Direct-to-Biology Accelerates PROTAC Synthesis and the Evaluation of Linker Effects on Permeability and Degradation. *ACS Med. Chem. Lett.* **2022**, *13* (7), 1182−1190.
(56) Osipyan, A.; Shaabani, S.; Warmerdam, R.; Shishkina, S. V.; Boltz, H.; Dömling, A. Automated, Accelerated Nanoscale Synthesis of Iminopyrrolidines. *Angew. Chem., Int. Ed.* **2020**, *59* (30), 12423−12427.
(57) Santiago, C. B.; Guo, J.-Y.; Sigman, M. S. Predictive and mechanistic multivariate linear regression models for reaction development. *Chem. Sci.* **2018**, *9* (9), 2398−2412.
(58) Lustosa, D. M.; Milo, A. Mechanistic Inference from Statistical Models at Different Data-Size Regimes. *ACS Catal.* **2022**, *12* (13), 7886−7906.
(59) Williams, W. L.; Zeng, L.; Gensch, T.; Sigman, M. S.; Doyle, A. G.; Anslyn, E. V. The Evolution of Data-Driven Modeling in Organic Chemistry. *ACS Cent. Sci.* **2021**, *7* (10), 1622−1637.

https://doi.org/10.1021/acscatal.3c04566
ACS Catal. 2023, 13, 16195−16206

(60) Shi, Y.; Prieto, P. L.; Zepel, T.; Grunert, S.; Hein, J. E. Automated Experimentation Powers Data Science in Chemistry. *Acc. Chem. Res.* **2021**, *54* (3), 546−555.
(61) Ahneman, D. T.; Estrada, J. G.; Lin, S.; Dreher, S. D.; Doyle, A. G. Predicting reaction performance in C−N cross-coupling using machine learning. *Science* **2018**, *360* (6385), 186−190.
(62) Newman-Stonebraker, S. H.; Smith, S. R.; Borowski, J. E.; Peters, E.; Gensch, T.; Johnson, H. C.; Sigman, M. S.; Doyle, A. G. Univariate classification of phosphine ligation state and reactivity in cross-coupling catalysis. *Science* **2021**, *374* (6565), 301−308.
(63) See Supporting Information.
(64) BTMG costs $244/5 mL from Millipore Sigma as of 12/7/2022.
(65) Sigman, M. S.; Harper, K. C.; Bess, E. N.; Milo, A. The Development of Multidimensional Analysis Tools for Asymmetric Catalysis and Beyond. *Acc. Chem. Res.* **2016**, *49* (6), 1292−1301.
(66) Grimme, S.; Bannwarth, C.; Shushkov, P. A Robust and Accurate Tight-Binding Quantum Chemical Method for Structures, Vibrational Frequencies, and Noncovalent Interactions of Large Molecular Systems Parametrized for All spd-Block Elements (Z = 1−86). *J. Chem. Theory Comput.* **2017**, *13* (5), 1989−2009.
(67) Bannwarth, C.; Ehlert, S.; Grimme, S. GFN2-xTB—An Accurate and Broadly Parametrized Self-Consistent Tight-Binding Quantum Chemical Method with Multipole Electrostatics and Density-Dependent Dispersion Contributions. *J. Chem. Theory Comput.* **2019**, *15* (3), 1652−1671.
(68) Grimme, S. Exploration of Chemical Compound, Conformer, and Reaction Space with Meta-Dynamics Simulations Based on Tight-Binding Quantum Chemical Calculations. *J. Chem. Theory and Comp.* **2019**, *15* (5), 2847−2862.
(69) Pracht, P.; Bohle, F.; Grimme, S. Automated exploration of the low-energy chemical space with fast quantum chemical methods. *Phys. Chem. Chem. Phys.* **2020**, *22* (14), 7169−7192.
(70) Zhao, Y.; Truhlar, D. G. The M06 suite of density functionals for main group thermochemistry, thermochemical kinetics, noncovalent interactions, excited states, and transition elements: two new functionals and systematic testing of four M06-class functionals and 12 other functionals. *Theor. Chem. Acc.* **2008**, *120* (1), 215−241.
(71) Ditchfield, R.; Hehre, W. J.; Pople, J. A. Self-Consistent Molecular-Orbital. IX. An Extended Gaussian-Type Basis for Molecular-Orbital Studies of Organic Molecules. *J. Chem. Phys.* **1971**, *54* (2), 724−728.
(72) Weigend, F.; Ahlrichs, R. Balanced basis sets of split valence, triple zeta valence and quadruple zeta valence quality for H to Rn: Design and assessment of accuracy. *Phys. Chem. Chem. Phys.* **2005**, *7* (18), 3297−3305.
(73) Glendening, E. D. B.; Badenhoop, J. K.; Reed, A. E.; Carpenter, J. E.; Bohmann, J. A.; Morales, C. M.; Landis, C. R.; Weinhold, F. *NBO 6.0*, 2008.
(74) Verloop, A. *Drug Design*, 1976, vol *III*; p 133.
(75) Brethomé, A. V.; Fletcher, S. P.; Paton, R. S. Conformational Effects on Physical-Organic Descriptors: The Case of Sterimol Steric Parameters. *ACS Catal.* **2019**, *9* (3), 2313−2323.
(76) Zell, D.; Kingston, C.; Jermaks, J.; Smith, S. R.; Seeger, N.; Wassmer, J.; Sirois, L. E.; Han, C.; Zhang, H.; Sigman, M. S.; Gosselin, F. Stereoconvergent and -divergent Synthesis of Tetrasubstituted Alkenes by Nickel-Catalyzed Cross-Couplings. *J. Am. Chem. Soc.* **2021**, *143* (45), 19078−19090.
(77) Wold, S. Validation of QSAR's. *Quant. Struct. -Act. Rel.* **1991**, *10* (3), 191−193.
(78) Golbraikh, A.; Tropsha, A. Beware of q2! *J. Mol. Graph. Model.* **2002**, *20* (4), 269−276.
(79) Gramatica, P. Principles of QSAR models validation: internal and external. *QSAR Comb. Sci.* **2007**, *26* (5), 694−701.
(80) Wold, S.; Dunn, W. J., III Multivariate quantitative structure-activity relationships (QSAR): conditions for their applicability. *J. Chem. Inf. Comp. Sci.* **1983**, *23* (1), 6−13.
(81) Hawkins, D. M. The Problem of Overfitting. *J. Chem. Inf. Comp. Sci.* **2004**, *44* (1), 1−12.
(82) Fan, M.; Zhou, W.; Jiang, Y.; Ma, D. Assembly of Primary (Hetero)Arylamines via CuI/Oxalic Diamide-Catalyzed Coupling of Aryl Chlorides and Ammonia. *Org. Lett.* **2015**, *17* (23), 5934−5937.
(83) Kumar, S. V.; Ma, D. Synthesis of N-(Hetero)aryl Carbamates via CuI/MNAO Catalyzed Cross-Coupling of (Hetero)aryl Halides with Potassium Cyanate in Alcohols. *J. Org. Chem.* **2018**, *83* (5), 2706−2713.
(84) Vitaku, E.; Smith, D. T.; Njardarson, J. T. Analysis of the Structural Diversity, Substitution Patterns, and Frequency of Nitrogen Heterocycles among U.S. FDA Approved Pharmaceuticals. *J. Med. Chem.* **2014**, *57* (24), 10257−10274.
(85) Dreher, S. D.; Krska, S. W. Chemistry Informer Libraries: Conception, Early Experience, and Role in the Future of Cheminformatics. *Acc. Chem. Res.* **2021**, *54* (7), 1586−1596.
(86) For a full list of Informer Aryl Halides and structures, see the Supplemental Information.
(87) We also attempted using our newly designed ligands **L28** and **L29** (Figure 4) to promote couplings to form products **3a**, **3w**, **3ab** and **3ad** (Figure 5b). But with limited preliminary data, we have yet to uncover an improvement in scope over **L4**. Our long term goal is to systematically study the scope of new ligands and hopefully develop substrate classification logic, for a recent example see: Samha, M.; Karas, L.; Vogt, D.; Odogwu, E.; Elward, J.; Crawford, J.; Steves, J.; Sigman, M. Predicting Success in Cu-Catalyzed C−N Coupling Reactions using Data Science. *ChemRxiv*, **2023**.
(88) Bogen, S. L.; Chen, P.; Clausen, D. J.; Hao, J.; Kalyani, D.; Rudd, M. T.; Walsh, S. P.; Wei, L.; Yang, D. Heteroaryl pyrrolidine and piperidine orexin receptor agonists and their preparation. WO2021026047, 2021.
(89) Yang, Q.; Zhao, Y.; Ma, D. Cu-Mediated Ullmann-Type Cross-Coupling and Industrial Applications in Route Design, Process Development, and Scale-up of Pharmaceutical and Agrochemical Processes. *Org. Process Res. Dev.* **2022**, *26* (6), 1690−1750.

https://doi.org/10.1021/acscatal.3c04566
ACS Catal. 2023, 13, 16195−16206